Electronic Supplementary Material (ESI) for Journal of Materials Chemistry A.

Supporting Information:

Pinhole-free hole transport layer significantly improves stability of $MAPbI_3$-based perovskite solar cells under operation conditions

Luis. K Ono‡, Sonia R. Raga‡, Mikas Remeika, Andrew J. Winchester,
*Atsushi Gabe, Yabing Qi**
Energy Materials and Surface Sciences Unit (EMSS), Okinawa Institute of Science and Technology Graduate University (OIST), 1919-1 Tancha Onna-son, Okinawa 904-0495 Japan.

‡These authors contributed to this work equally.
*E-mail: Yabing.Qi@OIST.jp

Contents:

10. Solvent contact angle measurements and physical properties of chloroform and chlorobenzene solvents. (Page 15)

Experimental section:

Transparent conductive substrates preparation. Fluorine-doped tin oxide coated on glass (FTO, Pilkington TEC7) was used as substrate. The FTO was etched and cleaned by brushing with an aqueous solution of sodium dodecyl sulfate, rinsing with milliQ water, sonication in 2-propanol and finally drying with N_2 gas. An 80 nm-thick TiO_2 compact layer was deposited by spray-pyrolisis using a 3:3:1 wt. mixture of acetylacetone, Ti (IV) isopropoxyde and anhydrous ethanol. Mesostructured TiO_2 layers of ~170 nm thickness was deposited by spin-coating a diluted paste (Dyesol, 90-T) in terpineol 1:3 wt. at 4000 rpm and subsequently sintered at 350 ºC for 10 min and 480 ºC for 30 min. After cooling down, the substrates were treated in UV-O_3 for 15 min and transferred in the N_2 glove box for perovskite deposition.

Perovskite film fabrication. Perovskite deposition was done following a modified two-step recipe.[1] First, a solution of PbI_2 in dimethylformamide (460 mg mL^{-1}) was prepared and left stirring at 70 ºC for at least 2 h. The solution was spin-coated on the mesostructured TiO_2 substrates, previously heated at 70 ºC, at 6000 rpm for 30 s. Before starting the spin-coating, the solution was left for 10s on the mesoporous layer for proper pore infiltration. After the spin coating, PbI_2 layer was dried at 70 ºC for 20 min. For the second step, a 20 mg mL^{-1} methylammonium iodide (MAI) solution in 2-propanol (IPA) was prepared and kept at 70 ºC. The PbI_2 films were dipped in the MAI solution during 30 s with gentle shaking of the substrate. After dipping, the substrates were rinsed in abundant IPA and dried immediately by spinning the sample using the spin-coater and annealed for 20 min on the hot plate at 70 ºC.

Solar cell fabrication. The solar cell device fabrication was completed by spin-coating a hole transport layer (HTM) that consists of a mixture of three materials: spiro-MeOTAD (2,2',7,7'-tetrakis(N,N-di-p-methoxy-phenylamine)-9,9'-spirobifluorene (Merck) dissolved in chlorobenzene (Wako, 032-07986) with 72.5 mg/mL concentration, 17.5 μL of Li-bis(trifluoromethanesulfonyl)-imide (LiTFSI, Sigma) dissolved in acetronitrile (52 mg/100 μL), and 28.8 μL of tert-butylpyridine (*t*-BP, Sigma) named ClB cells.[2,3] Additional batch of samples were prepared by only changing the chlorobenzene solvent to chloroform (Wako, 033-15721) generating pin-hole free HTL named ClF cells. Finally, the Au top electrodes (100 nm) were deposited by thermal evaporation through a shadow mask defining solar cell active areas of 0.05, 0.08, 0.12, and 0.16 cm^2.

Perovskite film characterization. The properties of the perovskite films were studied by x-ray diffraction (XRD, D8 Bruker), scanning electron microscope (SEM, FEI Quanta 250 FEG), and UV-visible spectroscopy (UV-vis, V-670 JASCO).

Perovskite solar cell characterization. Current-voltage device characteristics were measured by applying an external potential bias under standard 1 sun AM1.5G simulated solar irradiation (100 mW/cm^2, Newport Oriel Sol1A) and measuring the photocurrent generated (Keithley 2420 source meter).

Perovskite solar cell stability measurements. All as-prepared perovskite solar cells were first tested in Oriel solar simulator in air (RH ~ 50%) for the screening process. The cells with efficiencies above 10% were subsequently loaded in our home-designed environmental chamber coupled with a solar simulator (Peccell PEC-L01, AM1.5G) and two source meters (Keithley 2401) controlled by a LabView program allowing automatic sequential measurements on twenty four cells with adjustable acquisition time intervals. To simulate continuous solar cell operation an active bias voltage was applied to the cells maintaining the solar cell operation at the maximum power point (MPP). The switching between transient measurement and active BIAS was performed by an electronic board containing an array of relays (https://controlanything.com/Relay/Relay/CAT_RELAY24) and controlled by the home-written LabView code. For monitoring any eventual change of the light intensity over the stability measurement time an additional Si solar cell was mounted adjacent to the perovskite cells. In addition, a small humidity/temperature sensor (HIH6121-021-001, Honeywell) was mounted inside the environmental chamber. Home-written LabView code allowed periodic recording of humidity and temperature values during aging test. After the stability measurements post-mortem SEM images were performed using an FEI Helios G3 Dual Beam system on cells. SEM imaging used a beam energy of 3 keV and a current of 1.6 nA.

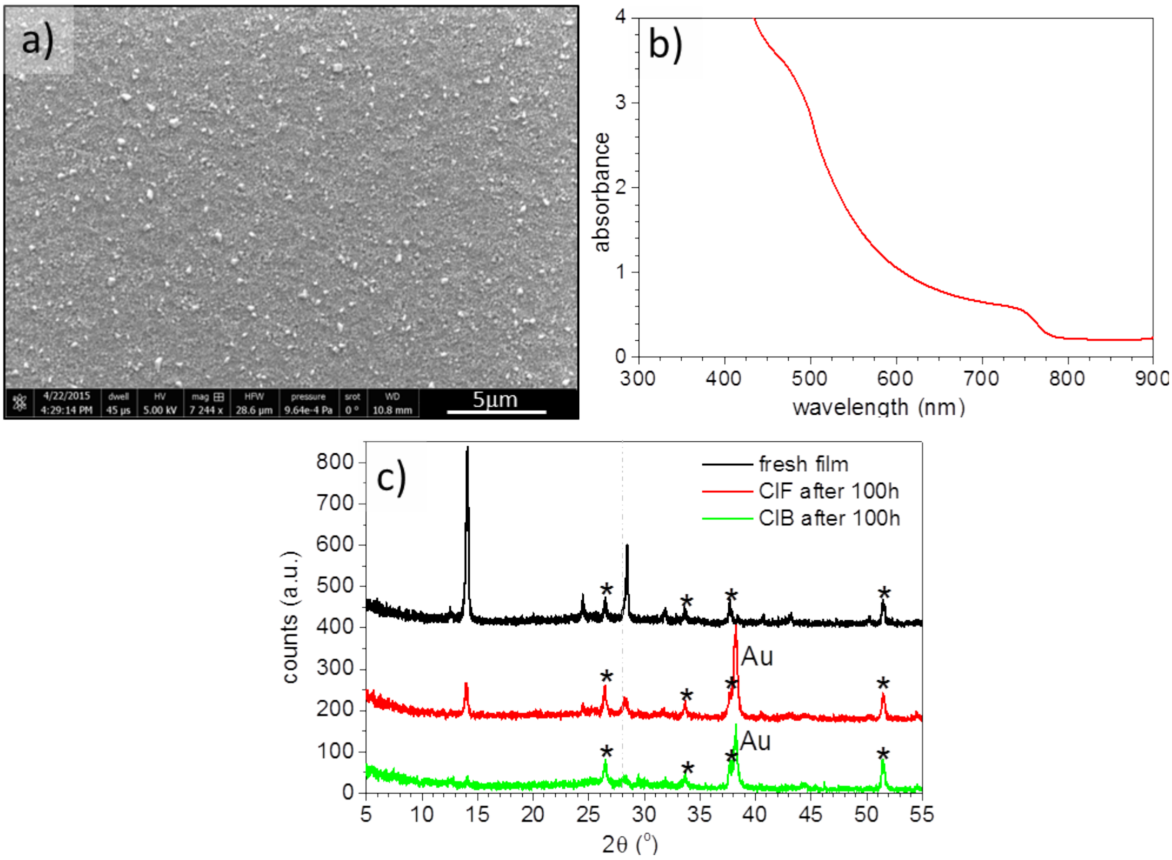

Figure S1. (a) SEM image of a FTO/mp-TiO_2/$MAPbI_3$ sample prepared by the two-step solution method. (b) UV-vis absorbance spectra of the fresh film, the onset of absorption at 781 nm corresponds to optical band gap of 1.58 eV. (c) XRD spectra of as-prepared perovskite film on mp-TiO_2 (black line). Red and green spectra correspond to ClF and ClB cells, respectively, acquired on the actual devices, after the 100 h stability test in air, under illumination and constant applied bias. The peaks with * were assigned to the FTO/TiO_2 substrate. Additional peak at 38° was assigned to top-Au contacts.

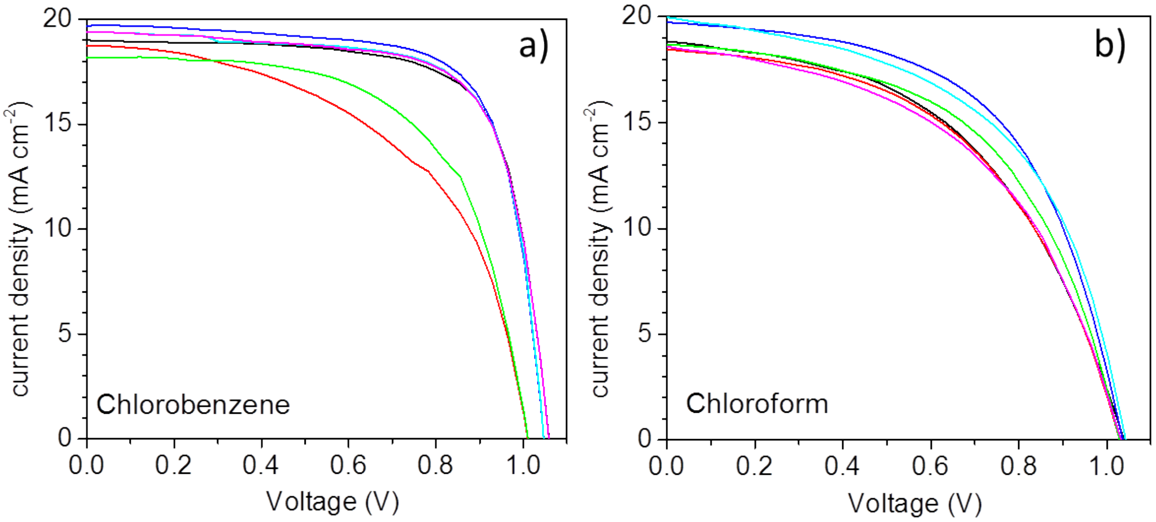

ClB	V_{oc} (mV)	j_{sc} (mA cm^{-2})	FF (%)	η (%)
Average	**1047 ± 22**	**19.2 ± 0.5**	**71.5 ± 8.1**	**14.5 ± 2.1**
champion	**1.047**	**19.7**	**72.1**	**14.9**

ClF	V_{oc} (mV)	j_{sc} (mA cm^{-2})	FF (%)	η (%)
Average	**1034 ± 5**	**18.7 ± 0.6**	**51.8 ± 2.7**	**9.9 ± 0.8**
champion	**1.036**	**19.7**	**55.8**	**11.4**

Figure S2. *j*-*V* curves from FTO/bl-TiO$_2$/mp-TiO$_2$/MAPbI$_3$/spiro-MeOTAD/Au devices with spiro-MeOTAD dissolved in (a) chlorobenzene (ClB cells) and (b) chloroform (ClF cells) irradiated under 1 sun (Oriel, AM1.5G) and measured with a scan rate of 0.37 V/s with 35 points scanned in the reverse direction, i.e. from 1.15 V to -0.1 V. The averaged solar cell parameters based on six cells and corresponding champion cell values are shown in the corresponding tables below the *j*-*V* plots.

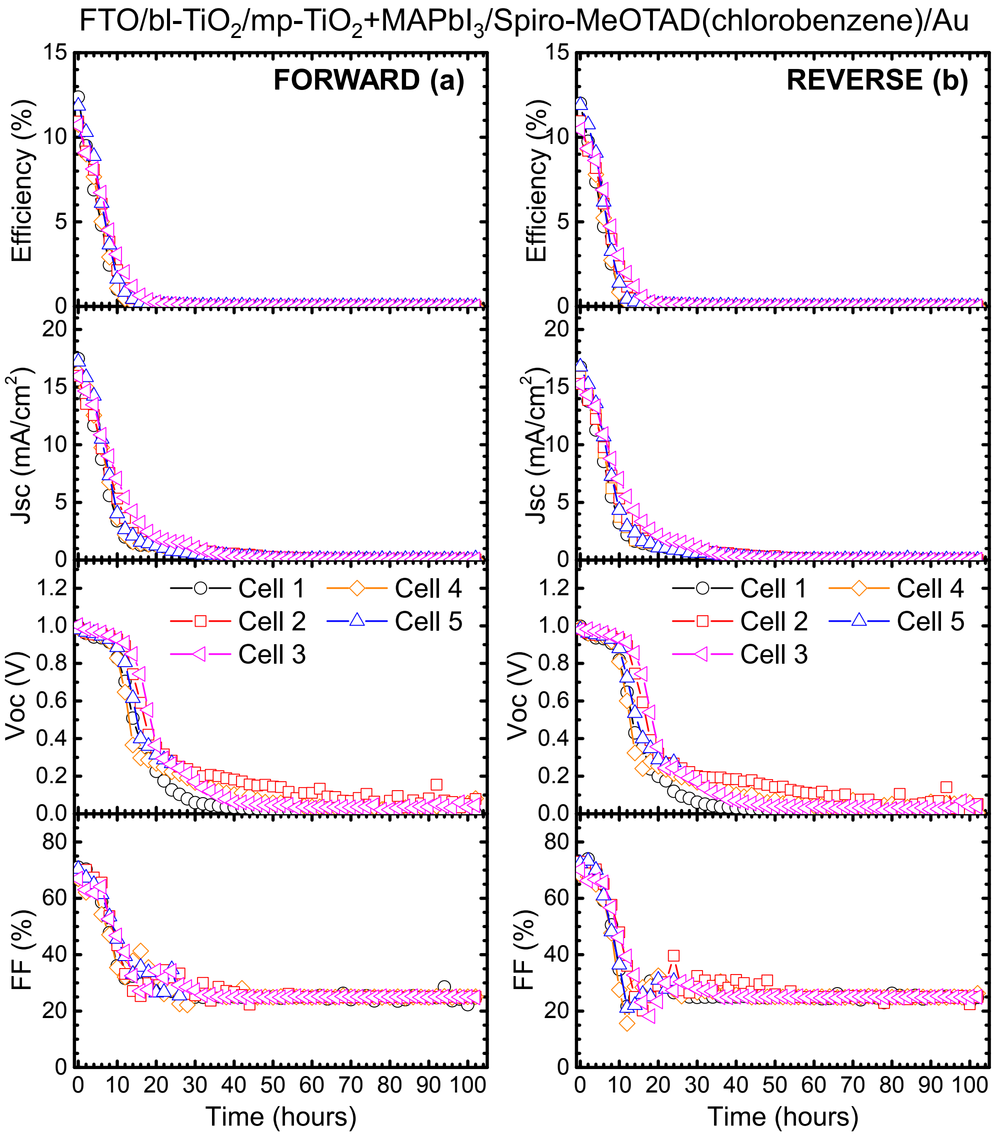

Figure S3. Steady-state efficiency, short circuit current (j_{sc}), open-circuit voltage (V_{oc}), and fill factor (*FF*) of individual cells in the $MAPbI_3$-based perovskite solar cell with spiro-MeOTAD layer prepared by chlorobenzene (ClB cells) and tested under air with controlled relative humidity of ~42%. When the cells were not under the *I-V* measurements a constant voltage were supplied to the cells matching the voltage at maximum power point.

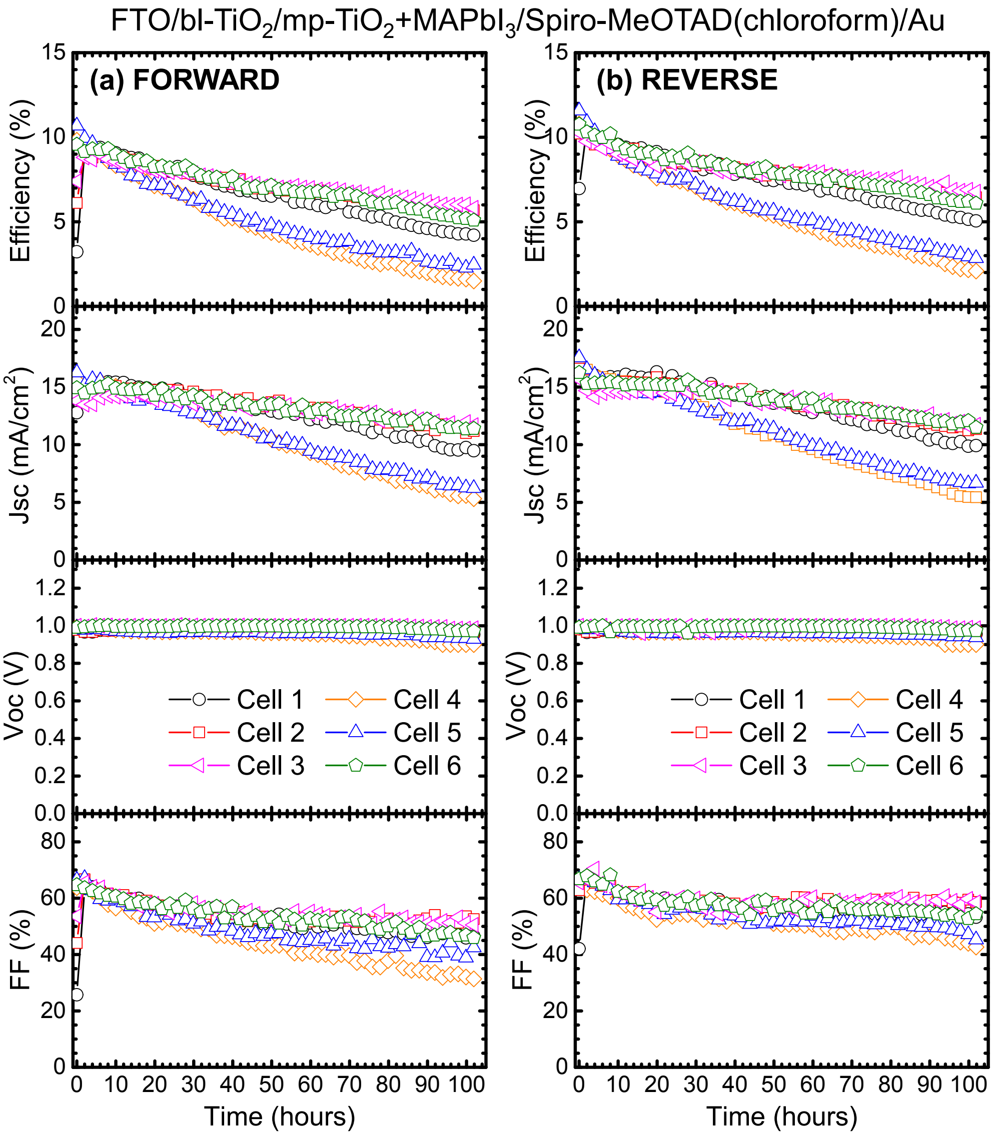

Figure S4. Steady-state efficiency, short circuit current (j_{sc}), open-circuit voltage (V_{oc}), and fill factor (FF) of individual cells in the MAPbI$_3$-based perovskite solar cell with spiro-MeOTAD layer prepared by chloroform (ClF cells) and tested under air with controlled relative humidity of ~42%. When the cells were not under the I-V measurements a constant voltage were supplied to the cells matching the voltage at maximum power point.

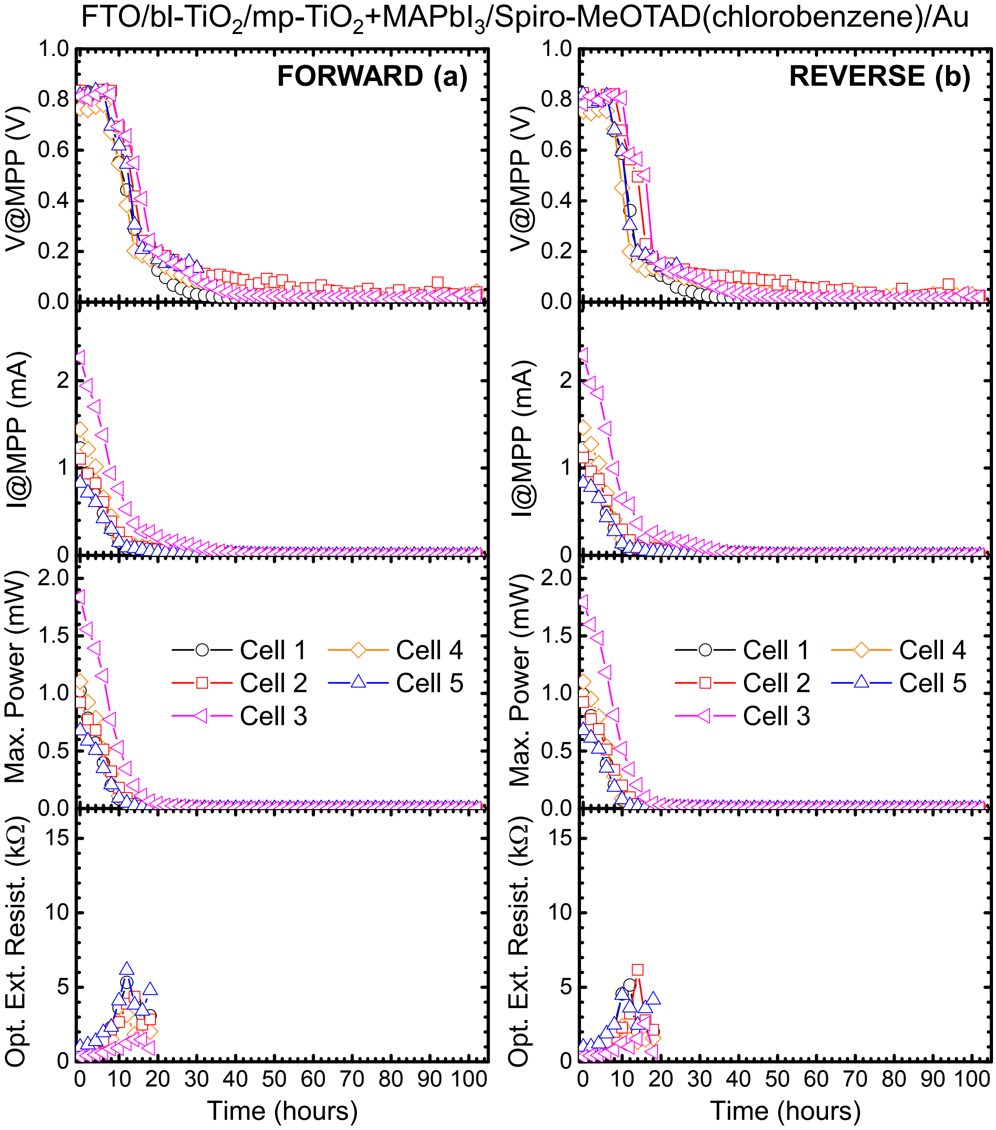

Figure S5. Solar cell electrical outputs of voltage and current corresponding at the maximum power point (V@MPP and I@MPP), generated maximum power (Max. Power), and cell optimum external resistance in $MAPbI_3$-based solar cells (ClB cells, Glass/FTO/bl-TiO_2/mp-TiO_2+$MAPbI_3$/spiro-MeOTAD-chlorobenzene/Au). Active load corresponding to the V@MPP was externally applied to maintain solar cell operation.

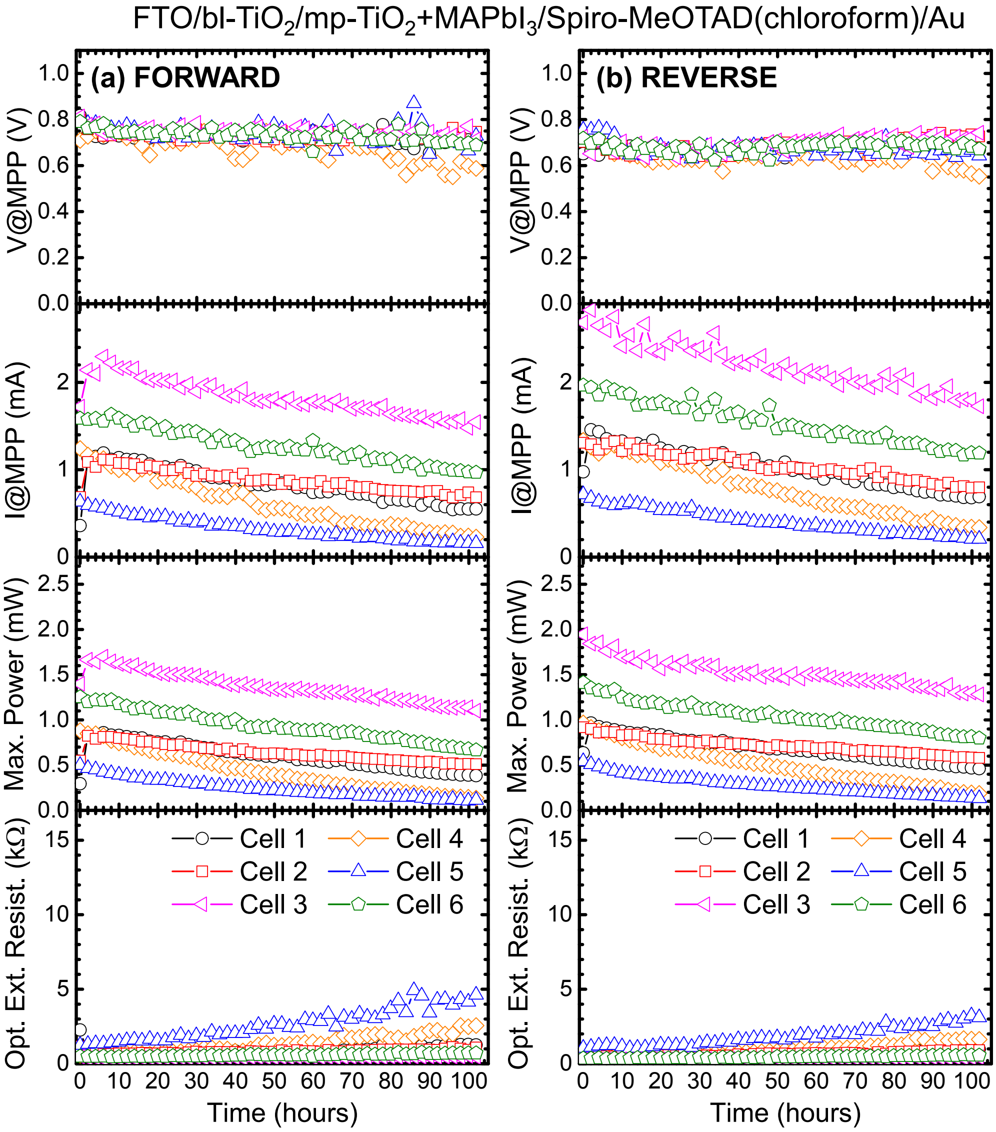

Figure S6. Solar cell electrical outputs of voltage and current corresponding at the maximum power point (V@MPP and I@MPP), generated maximum power (Max. Power), and cell optimum external resistance in MAPbI$_3$-based solar cells (ClF cells, Glass/FTO/bl-TiO$_2$/mp-TiO$_2$+MAPbI$_3$/spiro-MeOTAD-chloroform/Au). Active load corresponding to the V@MPP was externally applied to maintain solar cell operation.

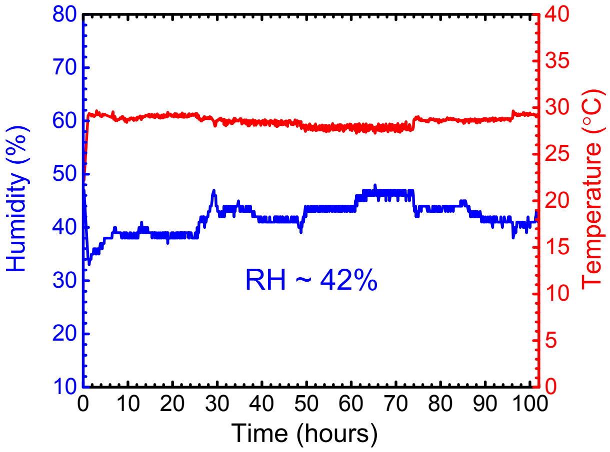

Figure S7. Relative humidity and temperature curves monitored during solar cell stability measurements performed in ambient air. The relative humidity and temperature near the cell were maintained at ~42% and ~28-29°C, respectively.

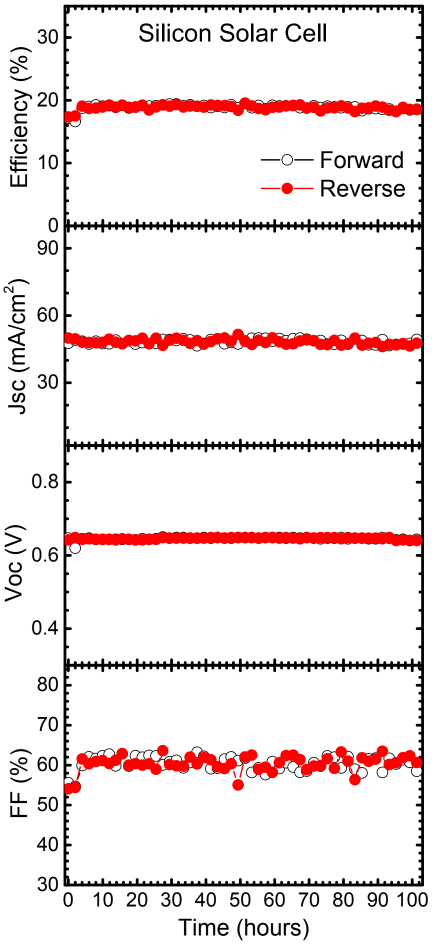

Figure S8. Solar cell parameters of a Si cell mounted adjacent to perovskite solar cells for monitoring any eventual changes in light intensity (AM1.5G) during the stability test. Changes in light intensity were typically negligible over the ~100 h stability test duration.

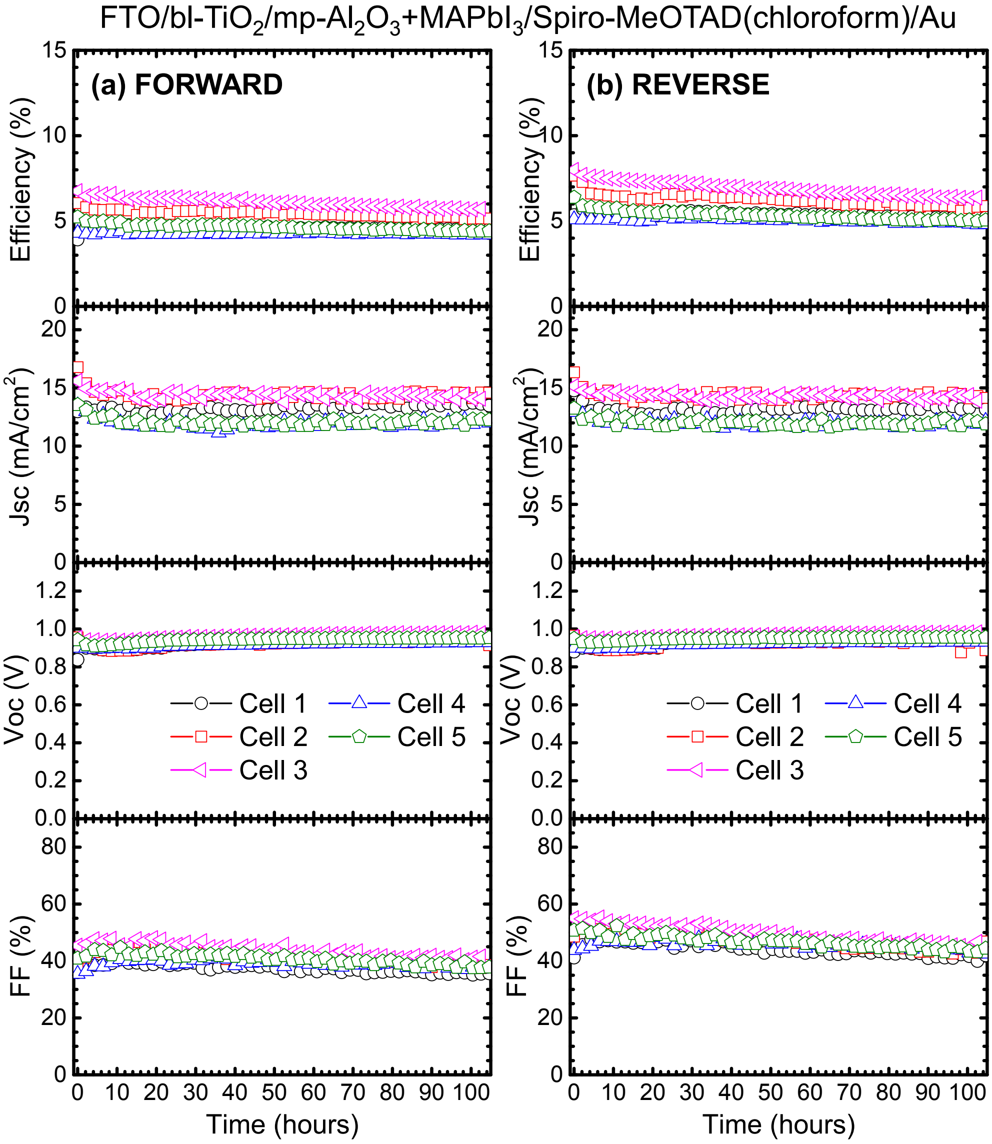

Figure S9. Steady-state efficiency, short circuit current (Jsc), open-circuit voltage (Voc), and fill factor (FF) of individual cells in the $MAPbI_3$-based perovskite solar cell with spiro-MeOTAD layer prepared by chloroform and tested in N_2 environment. When the cells were not under the I-V measurements a constant voltage were supplied to the cells matching the voltage at maximum power point.

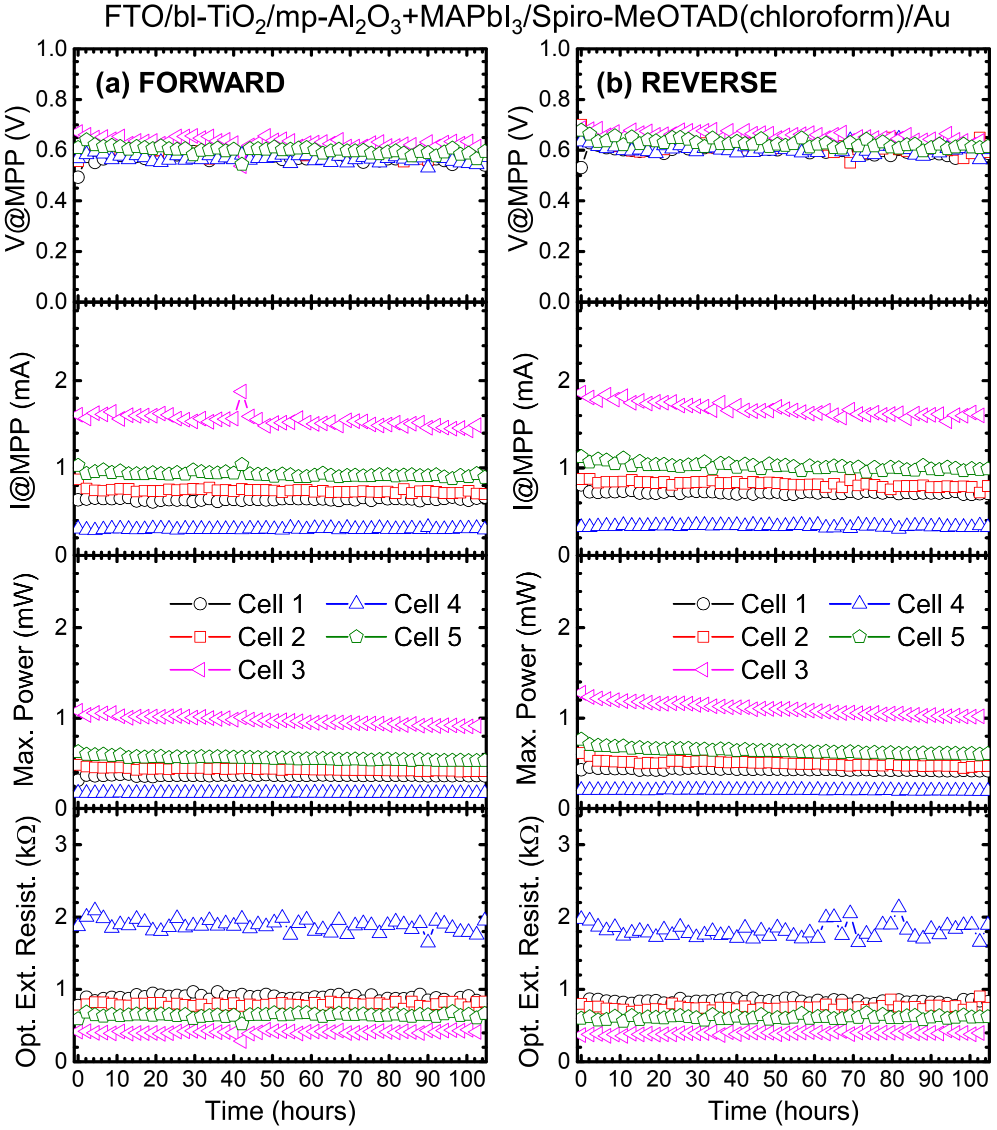

Figure S10. Solar cell electrical outputs of voltage and current corresponding at the maximum power point (V@MPP and I@MPP), generated maximum power (Max. Power), and cell optimum external resistance in $MAPbI_3$-based solar cells (Glass/FTO/bl-TiO_2/mp-Al_2O_3+$MAPbI_3$/spiro-MeOTAD-chloroform/Au). Active load corresponding to the V@MPP was externally applied to maintain solar cell operation.

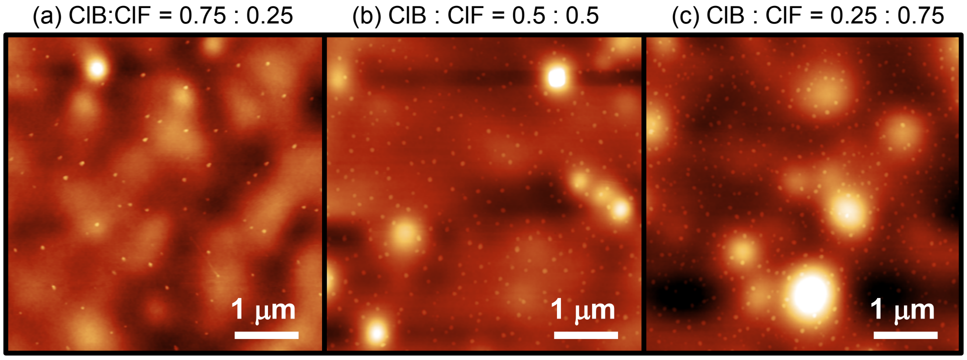

Figure S12. Tapping mode AFM topography images of spiro-MeOTAD HTL dissolved in mixed chlorobenzene:chloroform solvents with (a) 0.75:0.25, (b) 0.5:0.5, and (c) 0.25:0.75 volume ratios and spin-coated at 2000 rpm for 60 s on $MAPbI_3$/FTO substrates.

Figure S12 shows AFM images of spiro-MeOTAD HTL dissolved in different chlorobenzene:chloroform mixed solvents of 0.75:0.25, 0.5:0.5, and 0.25:0.75 volume ratios and spin-coated on $MAPbI_3$/FTO substrates. On those substrates a good film coating was observed and most likely associated with the good wettability of the solvents to the $MAPbI_3$ film, which were also confirmed by contact angle measurements (Figure S13). The new images show aggregates/crystallization (white spots) when mixed chlorobenzene:chloroform solvents are used to dissolve spiro-MeOTAD, Li-TFSI and t-BP. These small protrusions are observed to increase in density when increasing the chloroform:chlorobenzene ratio, Figure S12a-c. The pure ClB and pure ClF solutions were prepared to check reproducibility and spin coated on $MAPbI_3$ films. In the pure ClB sample, only holes are observed (similar to Figure 1a in the main texts) and in ClF films neither the bright protrusions nor pinholes can be detected (similar Figure 1b in the main texts). At present, it is not clear what causes the formation of aggregates and further experiments are necessary to provide insights.[4-6]

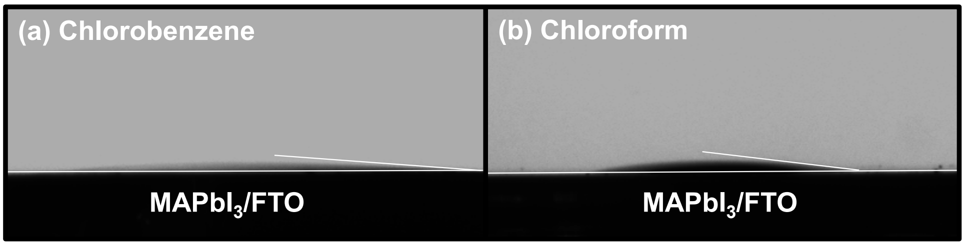

Figure S13. Photographic images of contact angle measurements after drop of (a) chlorobenzene and (b) chloroform solvent on the $MAPbI_3$/FTO samples. Contact angles of ~4º and ~7º were extracted from the images for chlorobenzene and chloroform droplets, respectively.

Solvents	Boiling point (°C)	Molecular weight (g/mol)	Vapor density (air=1)	Viscosity at 25 °C (mPa·s)
Chloroform	61.2	119.38	4.1	0.542
Chlorobenzene	132	112.56	9.3	0.753

Table S1. Comparison of physical properties of chloroform and chlorobenzene solvents used for dissolving the spiro-MeOTAD hole transport layer.

The fundamental aspects and mechanisms for the pinhole formation is complex and may involve multiple factors. The nature of the solvent such as the boiling point, dipole moment, viscosity, solubility of materials, spin-steps, spin-rate may affect the crystallinity and morphology of the prepared film.[4-13] For example, it has been pointed out previously that pinholes can form as a result of *localized dewetting* or *microbubbles* formed from degassing during the film drying process.[6,9] *Localized dewetting* can be caused by contaminants such as dust particles in the air or impurities in solvents [11]. The possibility of dewetting can be excluded in our studies because (1) the HTL deposition is performed inside the N_2 glove box located in the cleanroom environment; (2) high grade chlorobenzene and chloroform solvents were used in our experiments; (3) according to our surface tension measurements between solvents and $MAPbI_3$ solid films [13] (Figure S13†), the wettability of both chlorobenzene and chloroform solvents were very similar (with a small difference of ~3º), and both solvents were observed to spread well on the $MAPbI_3$ films. Therefore, the pinhole formation is more likely induced by the formation of *microbubbles*, which has been reported for solvents with high boiling points [8]. Solvents with high boiling points usually evaporate slowly during the spin-coating process generating microbubbles within the film during film drying [12]. In our studies, the boiling point of chlorobenzene (132°C) is significantly higher than that of the chloroform (61.2°C). The faster vaporization of chloroform may help solidify the spiro-MeOTAD film quickly without generating the pinholes.

References:

(1) Burschka, J.; Pellet, N.; Moon, S. J.; Humphry-Baker, R.; Gao, P.; Nazeeruddin, M. K.; Gratzel, M. Sequential deposition as a route to high-performance perovskite-sensitized solar cells. *Nature* **2013**, *499*, 316-319.

(2) Chen, Q.; Zhou, H.; Hong, Z.; Luo, S.; Duan, H.-S.; Wang, H.-H.; Liu, Y.; Li, G.; Yang, Y. Planar heterojunction perovskite solar cells via vapor-assisted solution process. *J. Am. Chem. Soc.* **2013**, *136*, 622-625.

(3) Liu, M. Z.; Johnston, M. B.; Snaith, H. J. Efficient planar heterojunction perovskite solar cells by vapour deposition. *Nature* **2013**, *501*, 395-398.

(4) Reisdorffer, F.; Haas, O.; Le Rendu, P.; Nguyen, T. P. Co-solvent effects on the morphology of P3HT:PCBM thin films. *Synth. Met.* **2012**, *161*, 2544-2548.

(5) Motaung, D. E.; Malgas, G. F.; Arendse, C. J. Comparative study: The effects of solvent on the morphology, optical and structural features of regioregular poly(3-hexylthiophene):fullerene thin films. *Synth. Met.* **2010**, *160*, 876-882.

(6) Birnie, D. P. A Model for Drying Control Cosolvent Selection for Spin-Coating Uniformity: The Thin Film Limit. *Langmuir* **2013**, *29*, 9072-9078.

(7) Kadem, B. Y.; Al-hashimi, M. K.; Hassan, A. K. The Effect of Solution Processing on the Power Conversion Efficiency of P3HT-based Organic Solar Cells. *Energy Procedia* **2014**, *50*, 237-245.

(8) Chen, K.-S.; Yip, H.-L.; Schlenker, C. W.; Ginger, D. S.; Jen, A. K. Y. Halogen-free solvent processing for sustainable development of high efficiency organic solar cells. *Org. Electron.* **2012**, *13*, 2870-2878.

(9) Stange, T. G.; Evans, D. F.; Hendrickson, W. A. Nucleation and Growth of Defects Leading to Dewetting of Thin Polymer Films. *Langmuir* **1997**, *13*, 4459-4465.

(10) Norrman, K.; Ghanbari-Siahkali, A.; Larsen, N. B. 6 Studies of spin-coated polymer films. *Annu. Rep. Prog. Chem. C* **2005**, *101*, 174-201.

(11) Kastner, C.; Muhsin, B.; Wild, A.; Egbe, D. A. M.; Rathgeber, S.; Hoppe, H. Improved phase separation in polymer solar cells by solvent blending. *J. Polym. Sci. B* **2013**, *51*, 868-874.

(12) Shaw, M.; Nawrocki, D.; Hurditch, R.; Johnson, D. Improving the process capability of SU-8. *Microsystem Technol.* **2003**, *10*, 1-6.

(13) Scriven, L. E. Physics and Applications of Dip Coating and Spin Coating. *Mat. Res. Soc. Symp. Proc.* **1988**, *121*, 717-729.